Atmos. Chem. Phys. Discuss., 15, 25433–25475, 2015
www.atmos-chem-phys-discuss.net/15/25433/2015/
doi:10.5194/acpd-15-25433-2015

Atmospheric Chemistry and Physics Discussions

Potential sensitivity of photosynthesis and isoprene emission to direct radiative effects of atmospheric aerosol pollution

S. Strada[1,a] **and N. Unger**[1]

[1]School of Forestry and Environmental Studies, Yale University, New Haven, CT, USA
[a]now at: Laboratoire des Sciences du Climat et de l'Environnement, Gif-sur-Yvette, France

Received: 16 July 2015 – Accepted: 8 August 2015 – Published: 17 September 2015

Correspondence to: S. Susanna (susanna.strada@lsce.ipsl.fr)

Published by Copernicus Publications on behalf of the European Geosciences Union.

Abstract

A global Earth system model is applied to quantify the impacts of direct anthropogenic aerosol effective radiative forcing on gross primary productivity (GPP) and isoprene emission. The impacts of different pollution aerosol sources (all anthropogenic, biomass burning and non-biomass burning) are investigated by performing sensitivity experiments. On the global scale, our results show that land carbon fluxes (GPP and isoprene emission) are not sensitive to pollution aerosols, even under a global decline in surface solar radiation (direct + diffuse) by ∼ 9 %. At the regional scale, plant productivity (GPP) and isoprene emission show a robust but opposite sensitivity to pollution aerosols, in regions where complex canopies dominate. In eastern North America and Europe, anthropogenic pollution aerosols (mainly from non-biomass burning sources) enhance GPP by +8–12 % on an annual average, with a stronger increase during the growing season (> 12 %). In the Amazon basin and central Africa, biomass burning aerosols increase GPP by +2–5 % on an annual average, with a peak in the Amazon basin during the dry-fire season (+5–8 %). In Europe and China, anthropogenic pollution aerosols drive a decrease in isoprene emission of −2 to −12 % on the annual average. Anthropogenic aerosols affect land carbon fluxes via different mechanisms and we suggest that the dominant mechanism varies across regions: (1) light scattering dominates in the eastern US; (2) cooling in the Amazon basin; and (3) reduction in direct radiation in Europe and China.

1 Introduction

Terrestrial gross primary productivity (GPP), the amount of carbon dioxide (CO_2) taken up every year from the atmosphere by plant photosynthesis, is the largest single flux in the carbon cycle and therefore plays a major role in global climate change. GPP is tightly connected to climatic variables (e.g., temperature, water, light) (Beer et al., 2010). In turn, terrestrial vegetation provides the main source of isoprene to

ACPD
15, 25433–25475, 2015

the atmosphere, which influences the loading of multiple short-lived climate pollutants and greenhouse gases (ozone, methane, secondary aerosols). Isoprene production is closely linked to plant photosynthesis (Pacifico et al., 2009; Unger et al., 2013). Hence, both GPP and isoprene emission may be influenced by a change in surface solar radiation (SSR, the sum of the direct and diffuse radiation incident on the surface) and surface atmospheric temperature (SAT). Anthropogenic aerosols affect directly the Earth's radiation flux via: (a) scattering, which alters the partitioning between direct and diffuse radiation and increases the diffuse fraction of SSR (Wild, 2009); and (b) absorption, which reduces SSR and SAT (Ramanathan et al., 2001). Furthermore, aerosols may attenuate indirectly SSR by acting as cloud condensation nuclei, thus perturbing cloud cover and cloud properties (Rosenfeld et al., 2008).

In 1991, Mount Pinatubo (Philippines) injected 20 megatons of sulfur dioxide (SO_2) into the stratosphere causing a massive production of sulfate aerosols, with substantial impacts on climate, and on the water and carbon cycles (Jones and Cox, 2001; Gu et al., 2003; Trenberth and Dai, 2007). In the aftermath of the eruption, a loss in net global radiation at the TOA (Top Of the Atmosphere) and a concomitant cooling were observed, and ultimately led to drying (Trenberth and Dai, 2007). By efficiently scattering light, the volcanic sulfate aerosol production caused a significant increase in diffuse solar radiation. In 1991 and 1992, at two northern mid-latitude sites, Molineaux and Ineichen (1996) recorded an increase in clear-sky diffuse radiation by +50 %, compensated by a concomitant decrease in direct radiation by −30 %. Over the same period, in a deciduous forest in North-America, Gu et al. (2003) ascribed to increased diffuse radiation an enhancement in plant productivity of +23 and +8 % in the two years following the Pinatubo eruption. On the global scale, enhancement in the terrestrial carbon sink was proposed as one of the main drivers of the sharp and rapid decline in the rate of atmospheric CO_2 rise observed in the post-Pinatubo period, which resulted in a decrease of 3.5 ppmv by 1995 in atmospheric CO_2 (Keeling et al., 1995; Jones and Cox, 2001; Gu et al., 2003). The "Mount Pinatubo experiment" suggested a possible global response of terrestrial vegetation to the "diffuse fertilization effect" (DFE).

ACPD
15, 25433–25475, 2015

Observational and theoretical studies show that plant productivity is more efficient under multi-directional diffuse rather than direct light because shaded non-light-saturated leaves increase their photosynthetic rate (Gu et al., 2002).

The DFE on plant photosynthesis has been extensively observed at ecosystem scale under cloudy skies (e.g., Gu et al., 2002; Niyogi et al., 2004; Cheng et al., 2015) and a chronic aerosol loading (e.g., Gu et al., 2003; Oliveira et al., 2007; Cirino et al., 2014) in diverse ecosystems (rainforest, deciduous and needleleaf forest, crop- and grasslands). The main conclusions of these studies are: (1) DFE prevails in complex and closed canopies, such as forests (Niyogi et al., 2004; Kanniah et al., 2012); (2) intermediate aerosol optical depth (AOD) enhances plant productivity, while high AOD (> 2–3) reduces carbon uptake rate because of a large reduction in direct radiation (Oliveira et al., 2007; Artaxo et al., 2013; Cirino et al., 2014). An ecosystem-scale measurement study in a European mixed needleleaf and deciduous forest reported increased isoprene emissions under conditions of higher diffuse light (Laffineur et al., 2013).

A few modeling studies have investigated aerosol-induced effects on plant productivity. Regional- and daily-scale assessments have been performed over: the Yellow River region (China), selecting a period of five days (Steiner and Chameides, 2005); and over the eastern US, selecting two growing seasons (Matsui et al., 2008). Results in both studies are consistent with the main conclusions of the local observational studies. Steiner and Chameides (2005) demonstrated the importance of both aerosol-induced radiative (i.e., change in light amount and its partitioning) and thermal (i.e., change in surface temperature) effects on plant transpiration and productivity. However, these studies focus on short time periods and a limited number of ecosystems using offline models with single-layer canopy schemes.

By applying a multy-layer canopy scheme in the framework of an offline modeling setup (i.e., aerosol, radiative transfer and land use models are coupled offline), Rap et al. (2015) performed a regional- and decade-scale assessment of aerosol-induced effects on plant productivity in the Amazon basin from 1998 to 2007. The authors specifically focused on biomass burning aerosols (BBAs) and quantified that BBAs in-

ACPD
15, 25433–25475, 2015

crease the annual mean diffuse light and net primary production (NPP) by, respectively, ~ 5 and ~ 2.5 %. Deforestation fires play a key role and drive ~ 40 % of the estimated changes in light and photosynthesis. Moreover, Rap et al. (2015) assessed that in the Amazon basin during 1998–2007 the DFE (a) was larger than the CO_2 fertilization effect, and (b) it could counteract the negative effect of droughts on land carbon fluxes.

A global-scale assessment of the aerosol-induced effects on the carbon cycle was performed by Mercado et al. (2009) using an offline land-surface model (with a multi-layer canopy scheme). The authors concluded that DFE enhanced the global land carbon sink by +23.7 % over the 20th century. Mercado et al. (2009) reconstructed historical SSR using radiative transfer calculations and a global climate dataset for the "global dimming" (period 1950–1980) and the "global brightening" period (after 1990s) (Wild, 2009, 2012; Streets et al., 2009). Recently, Chen and Zhuang (2014) applied an atmospheric radiative transfer module coupled with a terrestrial ecosystem module to quantify aerosol direct radiative effects on global terrestrial carbon dynamics during 2003–2010. Using transient atmospheric CO_2 and prognostic leaf area index (LAI, one-sided green leaf area per unit ground area), the authors evaluated aerosol impacts on plant phenology, thermal and hydrological conditions as well as solar radiation. Chen and Zhuang (2014) estimated that, on a global scale, aerosols enhance GPP by 4.9 $Pg\,C\,yr^{-1}$ and slightly affect respiration. Chen and Zhuang (2014) accounted for all atmospheric aerosols and they did not target anthropogenic pollution aerosols.

Understanding all anthropogenic factors that influence the land carbon cycle is crucial to better manage terrestrial vegetation and to any effort to mitigate climate change by stabilizing atmospheric CO_2 concentrations. In the present study, we quantify the sensitivity of GPP and isoprene emission to the direct radiative effects of a realistic present-day pollution aerosol loading. Using a global Earth system model that represents vegetation–oxidant–aerosol–climate coupling, we perform sensitivity simulations to isolate the impact of the present-day pollution aerosols on GPP and isoprene emission. We tackle the direct aerosol effect only (absorption + scattering) and its impact on SSR and SAT that affects land carbon fluxes. Aerosol indirect effects on cloud prop-

ACPD
15, 25433–25475, 2015

erties are not addressed in this study due to the large uncertainties (Boucher et al., 2013; Myhre et al., 2013a). This study focuses on GPP because it is the first step in the long-term storage of atmospheric CO_2 in the living tissues of plants and is directly affected by solar radiation. We do not address aerosol effects on other land carbon cycle fluxes (e.g., respiration, net ecosystem exchange). We employ the effective radiative forcing (ERF) concept metric introduced in the IPCC AR5 in which all physical variables are allowed to respond to the direct aerosol–radiation perturbations except for those concerning the ocean and sea ice (Myhre et al., 2013b). The inclusion of these rapid adjustments in the ERF metric allows us to investigate the multiple short-term aerosol-induced concomitant meteorological impacts on the biosphere.

Section 2 describes the global Earth system model tool (NASA ModelE2-YIBs) and the experimental design. In Sect. 3, we evaluate simulated present-day atmospheric aerosols and GPP against global observational datasets including AOD from the Moderate Resolution Imaging Spectroradiometer (MODIS) and global gridded GPP that was generated using data orientated diagnostic upscaling of site-derived GPP from FLUXNET (Beer et al., 2010; Bonan et al., 2011; Jung et al., 2011). In addition, we present the analysis of results from the sensitivity simulations. In Sect. 4 we discuss the results and summarize conclusions.

2 Methodology

2.1 Global Earth system model: NASA ModelE2-YIBs

We apply the NASA GISS ModelE2 global chemistry-climate model at $2^\circ \times 2.5^\circ$ latitude by longitude horizontal resolution with 40-vertical layers extending to 0.1 hPa (Schmidt et al., 2014). The Yale Interactive Terrestrial Biosphere Model (YIBs) is embedded inside NASA ModelE2 in a framework known as NASA ModelE2-YIBs (Unger et al., 2013). The global climate model provides the meteorological drivers for the vegetation physiology. The land-surface hydrology submodel provides the grid cell level

ACPD
15, 25433–25475, 2015

soil characteristics to the vegetation physiology. The model framework fully integrates the land biosphere–oxidant–aerosol system such that these components interact with each other and with the physics of the climate model. On-line oxidants affect aerosol production and on-line aerosols provide surfaces for chemical reactions and influence photolysis rates. The chemistry and aerosol schemes and their coupling have been well documented and extensively compared with observations and other global models (e.g., Bell et al., 2005; Bauer et al., 2007; Koch et al., 2006; Koch and Del Genio, 2010; Unger, 2011; Myhre et al., 2013a; Shindell et al., 2006, 2013a, b; Stevenson et al., 2013).

The aerosol package includes mass-based simulation of sulfate, nitrate and sea salt (e.g., Koch et al., 2006), carbonaceous aerosols (black carbon, BC, and primary organic matter, OC) (Koch and Hansen, 2005), mineral dust (Miller et al., 2006), and biogenic secondary organic aerosol (BSOA) (Tsigaridis and Kanakidou, 2007). The model assumes log-normal size distributions with effective radii: 0.2 µm (sulfate); 0.3 µm (nitrate); 0.1 µm (BC); 0.3 µm (OC). Sea salt aerosols are represented by two size bins with effective radii of 0.44 and 5 µm. Mineral dust aerosols are tracked in four size bins, ranging from 0.1 to 10 µm, and can be coated by sulfate and nitrate aerosols. Hygroscopic aerosols (sulfates, nitrates, sea salt and organic carbon) increase in size as the relative humidity increase, which increases the aerosol scattering efficiency and radiative forcing (Schmidt et al., 2006).

The direct effect interaction between aerosols and radiation is reproduced by the on-line (two-way coupled) mode: aerosol fields are simulated at each model time step (30 min) and influence the simulated short and longwave radiation through scattering and absorption in the radiation submodel, which in turn influences the climate dynamics. Thus, aerosols induce (a) changes in simulated diffuse and direct photosynthetically active radiation (PAR, spectral range of surface visible solar radiation, 400–700 nm, used by plants to photosynthesize) that are passed from the radiation submodel to the vegetation model; and (b) fast feedback changes in meteorology (tem-

ACPD
15, 25433–25475, 2015

perature, precipitation, circulation) that are passed from the model's atmosphere to the vegetation model.

The Yale Interactive Terrestrial Biosphere model (YIBs)

The vegetation structure describes eight plant functional types (PFTs): tundra, grassland, shrubland, deciduous broadleaf forest, savannah, tropical rainforest, evergreen needleleaf forest, and cropland. The PFT-specific vegetation cover fraction and LAI are the standard atlas-based distribution in NASA GISS ModelE2 (Schmidt et al., 2014). Leaf area index (LAI) for each PFT is prescribed according to regular seasonal sinusoidal variation between PFT-specific minimum and maximum seasonal LAI values that is insensitive to climate drivers or carbon balances (Rosenzweig and Abramopoulos, 1997; Friend and Kiang, 2005). Each model PFT fraction in the vegetated part of each grid cell represents a single canopy. The canopy radiative transfer scheme assumes a closed canopy and distinguishes vertically canopy layers into sunlit and shaded leaves, as well as the different contribution from direct and diffuse PAR (from the climate model's radiation scheme) at the leaf level (Spitters et al., 1986). The leaf-level carbon and water fluxes are scaled up to the canopy level by integrating over each canopy layer, using an adaptive number of layers (typically 16) (Friend and Kiang, 2005). After upscaling from leaf to canopy, the carbon and water fluxes are exchanged with the atmosphere on the 30 min physical integration time step of the global climate model.

The vegetation biophysical fluxes are calculated using the well-established Michealis–Menten enzyme-kinetics leaf model of photosynthesis (Farquhar et al., 1980; Von Caemmerer and Farquhar, 1981) and the stomatal conductance model of Ball and Berry (Collatz et al., 1991). In the leaf model, the rate of net CO_2 uptake in the leaves of C_3 plants is the result of three competing processes: J_c, the carboxylation-limited rate; J_e, the electron transport-limited photosynthesis rate; and J_s, the export-limited rate to use photosynthesis products. The coupled photosynthesis and stomatal conductance equations are solved analytically at the leaf level using a cubic function in

ACPD
15, 25433–25475, 2015

net photosynthetic rate. Isoprene emission is calculated as a function of J_e, intercellular and atmospheric CO_2 and canopy temperature (Unger et al., 2013).

This version of the land carbon cycle model captures the meteorological (light, temperature, relative humidity, precipitation) responses of photosynthesis. The use of fixed canopy structures and phenology means that leaf mass is not driven by photosynthetic uptake of CO_2 and a closed carbon cycle is not simulated. Thus, the simulated GPP and isoprene emission responses may be underestimated because the LAI is insensitive to CO_2 uptake and climate.

2.2 Simulations

The atmosphere-only configuration of NASA ModelE2-YIBs is used to perform a control simulation ("SimCTRL") representative of the present-day (~2000s). Prescribed decadal average monthly-varying sea surface temperature (SST) and sea ice observations for 1996–2005 from the HadSST dataset (Rayner et al., 2006) provide the lower boundary conditions for the global climate model. The present day trace gas and aerosol emissions are prescribed to year 2000 values from the historical inventory developed for IPCC AR5 (RCP4.5; Lamarque et al., 2010). Atmospheric levels of long-lived greenhouse gases are prescribed to: CO_2 = 370 ppmv; CH_4 = 1733 ppbv in Southern Hemisphere and 1814 ppbv in Northern Hemisphere; N_2O = 316 ppbv. A set of three sensitivity perturbation simulations is performed that selectively remove anthropogenic short-lived gas-phase precursor and primary aerosol emissions: (a) all anthropogenic emissions including biomass burning ("SimNOant"), (b) biomass burning emissions only ("SimNObb"), and (c) industrial emissions ("SimNOind", all anthropogenic emissions are removed except biomass burning emissions).

The control and sensitivity simulations are run for 32 model years recycling the year 2000 boundary conditions every year but allowing the changes in atmospheric aerosol composition to influence meteorology and the land biosphere. By prescribing SSTs and sea ice cover at climatological values, while letting all other physical components of the Earth system to respond until reaching steady state, we capture short-term response

ACPD
15, 25433–25475, 2015

of land surface climate to aerosol radiation perturbation. This fixed-SST technique allows us to compute ERF, the forcing metric that accounts for rapid tropospheric adjustments and better characterizes drivers in the troposphere (e.g., aerosols) (Myhre et al., 2013b). Hence, the fixed-SST technique enables us to analyze multiple meteorological effects of the direct aerosol–radiation interactions. The long run-time is necessary to allow the fast land and atmosphere climatic feedbacks to respond to the aerosol perturbations and the TOA radiation fluxes to equilibrate. The first 12 model years are discarded as spin-up. The last 20 years of each simulation are used for analysis. Our goal is to isolate the effects of aerosol pollution on the land biospheric fluxes. Therefore, we compute the absolute differences in X variable as: $\Delta X = X_{\mathrm{ctrl}} - X_{\mathrm{sens}}$. Percentage changes in X are calculated relative to the control experiment (i.e., $\Delta_{\%}X = \Delta X / X_{\mathrm{ctrl}} \times 100$) and are illustrated in the Supplement.

3 Results

3.1 Evaluation of present-day control simulation

Present-day values of global mean aerosol column burden and ERF for aerosol–radiation interaction by component shown in Table 1 are consistent with ranges presented in the IPCC AR5 report (Boucher et al., 2013; Myhre et al., 2013b). Similarly the present-day land carbon fluxes are in good agreement with previous estimates (Table 2). Simulated global annual GPP (116.0 $\mathrm{Pg\,C\,yr^{-1}}$) is in reasonable agreement with current understanding of the present-day carbon cycle budget (based on FLUXNET: 123 ± 8 $\mathrm{Pg\,C\,yr^{-1}}$, Beer et al., 2010; based on MODIS: 109.29 $\mathrm{Pg\,C\,yr^{-1}}$, Zhao et al., 2005; based on the Eddy Covariance-Light Use Efficiency model: 110.5 ± 21.3 $\mathrm{Pg\,C\,yr^{-1}}$, Yuan et al., 2010). The global isoprene source is 402.8 $\mathrm{Tg\,C\,yr^{-1}}$ and agrees with previous global estimates (400–700 $\mathrm{Tg\,C\,yr^{-1}}$, Guenther et al., 2006; 412–601 $\mathrm{Tg\,C\,yr^{-1}}$, Arneth et al., 2008).

ACPD
15, 25433–25475, 2015

3.1.1 Aerosol Optical Depth (AOD)

We use the quality assured Terra MODIS Collection 5 (C5.1) monthly mean product (Level 3), a globally gridded dataset at $1^\circ \times 1^\circ$ resolution regridded to at $2^\circ \times 2.5^\circ$ resolution for comparison with the global model. To infer clear-sky (non cloudy) aerosol properties in part of the visible and shortwave infrared spectrum, MODIS C5.1 relies on two algorithms depending on surface reflectance: (1) the Dark Target (DT) algorithm, under conditions of low surface reflectance (e.g., over ocean, vegetation) (Levy et al., 2010); (2) the Deep Blue (DB) algorithm, designed to work under high surface reflectance, such as over desert regions (Hsu et al., 2004; Shi et al., 2014). To cover both dark and bright surfaces, we merge the DT and DB AOD products (i.e., DT missing data are filled in with DB values). We use MODIS TERRA C5.1 AOD data from 2000 to 2007 because DB AOD data are only available for this period due to calibration issues (Shi et al., 2014). The MODIS instrument also measures the fine model weighting (ETA) at 550 nm, consequently the fine-mode AOD can be computed as: fine-AOD = AOD × ETA, where fine-AOD is a fraction of the AOD contributed by fine mode sized particles (i.e., effective radius $\ll 1.0\,\mu m$) (Levy et al., 2010; Bian et al., 2010). Quantitative use of MODIS fine-AOD is not appropriate because fine-mode aerosols play a main role in the scattering process (Levy et al., 2010).

NASA ModelE2-YIBs provides separately all-sky and clear-sky AOD diagnostics; we focus on clear-sky output since that is more comparable to the spaceborne observations. The model coarse-mode AOD (PM_{10}, atmospheric particulate matter with diameter $< 10\,\mu m$) includes all simulated aerosol species (sulfate, nitrate, organic and black carbon, SOA, sea salt and mineral dust); the model fine-mode AOD ($PM_{2.5}$, atmospheric PM with diameter $< 2.5\,\mu m$) accounts for all simulated aerosol species except sea salt and dust.

Figure 1 compares the spatial distribution of annual and seasonal (boreal summer and winter) mean coarse-mode AOD in NASA ModelE2-YIBs (control present-day simulation) with observations from the MODIS satellite instrument (averaged over 2000–

ACPD
15, 25433–25475, 2015

2007). Model global mean coarse-mode AODs are consistent with MODIS AOD global means. NASA ModelE2-YIBs reproduces strong biomass burning and dust episodes over Africa. In contrast, on both annual and seasonal averages the model underestimates the thickness of the aerosol layer over China and India, which is likely related to dust. The model's underestimate of Asian dust should not influence the focus of this study, to assess the impacts of anthropogenic pollution aerosols on the land carbon fluxes. The spatial and temporal distribution of fine-mode aerosols in NASA ModelE2-YIBs is consistent with MODIS observations (Fig. 2). In general, the model shows a slightly higher fine-aerosol layer compared to MODIS, e.g., over Europe, India and South America. Over China, model fine-AOD distribution is consistent with MODIS on the annual average; however, the model does not show the seasonal variability that MODIS observes.

3.1.2 Gross Primary Productivity (GPP)

In Fig. 3, we compare the spatial distribution of annual and seasonal (boreal summer and winter) mean GPP in NASA ModelE2-YIBs model (control present-day simulation) with a global FLUXNET-derived GPP product (averaged over 2000–2011). The model is consistent with the broad spatio-temporal variability in FLUXNET-derived GPP. We find a weaker annual and seasonal signal in the model GPP over the cerrado area in central South-America.

3.2 Aerosol-induced changes to surface meteorology

Table 1 shows the changes in aerosol column burden (ACB) and ERF for each sensitivity simulation. Removal of all anthropogenic emissions (SimNOant): (a) reduces by $\sim$ 10 % sulfate column burden and ERF; (b) decreases by $\sim$ 70–80 % nitrate and SOA column burden and reduces respectively by $\sim$ 80 and $\sim$ 60 % sulfate and SOA ERF; and (c) reduces nearly to zero both column burden and ERF of OC and BC. Removal of biomass burning emissions (SimNObb) results in (a) negligible column burden and

ACPD
15, 25433–25475, 2015

ERF from OC and BC, (b) reduction by ∼ 30 % on both nitrate ACB and ERF; and (c) no impacts on the other aerosol components. Removal of anthropogenic emissions except biomass burning emissions (SimNOind): (a) has the same effect of SimNOant on sulfate burden and ERF; (b) decreases by ∼ 70 % nitrate column burden and ERF; (c) reduces nearly to zero both column burden and ERF of industrial OC and BC; and (d) decreases by ∼ 30 % both ACB and ERF of SOA. Above-listed changes in the aerosol burden ultimately affect solar radiation, temperature and relative humidity (RH) at the Earth's surface, as we explore below.

3.2.1 Surface solar radiation

The global annual average shortwave visible solar radiation (total, direct and diffuse) for each simulation are reported in Table 2. Hereafter, we shorten "shortwave visible solar radiation" to "radiation". Global total and diffuse radiation are slightly affected by the pollution aerosol burden, and their changes have opposite sign but similar value (percentage changes range from 1.7 to 2.5 %); on the contrary, direct radiation is highly sensitive to change in the aerosol burden (percentage change spans from 3.6 to 11.2 %) (Table 2). Referred to present-day conditions, anthropogenic emissions drive a decrease in global total and direct radiation by, respectively, −2.3 % ($-5.2\,W\,m^{-2}$) and to −11.2 % ($-9.0\,W\,m^{-2}$), while global diffuse radiation increases by +2.5 % ($+3.7\,W\,m^{-2}$). Biomass burning emissions have almost zero effects on global total and diffuse radiation, while they reduce direct radiation by −3.6 % ($-2.9\,W\,m^{-2}$). Non-biomass burning emissions (industry, power generation, road vehicles) decrease global total radiation by −1.7 % ($-3.8\,W\,m^{-2}$) and increase global diffuse radiation by the same percentage (absolute change: $+2.6\,W\,m^{-2}$), while global direct radiation reduces by −8 % ($-6.4\,W\,m^{-2}$).

Anthropogenic aerosol burden affect globally annual average radiation (total, direct and diffuse) at the Earth's surface (Fig. 4). Under the aerosol laden due to anthropogenic pollution, total and direct radiation decrease, while diffuse radiation rises. Via light absorption and scattering, anthropogenic aerosols drive a significant decrease

ACPD
15, 25433–25475, 2015

in total and direct radiation by, respectively, −12 to −20 W m^{-2} (−10 to −20 %) and by −20 to −36 W m^{-2} (−20 to −40 %) over industrialized (eastern North America, Europe and Asia) and biomass burning (the Amazon basin and central Africa) regions (Fig. 4a–b). Over these regions, via light scattering, anthropogenic aerosols increase diffuse radiation by +6–20 W m^{-2} (+6–12 %). Among industrialized regions, the eastern US shows the largest increase in diffuse radiation (+8–20 W m^{-2}; +8–12 %), most likely due to sulfate and BSOA production that characterize this region (e.g., Carlton et al., 2010; Ford and Heald, 2013) (Fig. 4c). Biomass burning aerosols drive a decrease in total radiation of −12 to −28 W m^{-2} (−10 to −20 %) in the Amazon basin and central Africa, and a weaker decrease of −6 to −12 W m^{-2} (−5 to −10 %) over boreal regions (Canada and Eurasia) (Fig. 4d). Diffuse radiation increases with a larger signal over central Africa (+8–12 W m^{-2}; +8–10 %) compared to the Amazon basin (+6–8 W m^{-2}; +8–10 %) (Fig. 4f). Changes in total and diffuse radiation are localized over the main biomass burning regions (the Amazon basin, Africa, South-East Asia and boreal regions), while decrease in direct radiation also affect robustly minor biomass burning regions such as North America and Australia (Fig. 4e). Pollution aerosols from non-biomass burning sources are responsible of a strong reduction in total and direct radiation over Europe and China (Fig. 4g and h).

During boreal summer, aerosol-induced impacts on solar radiation amplify over aerosol-source regions, such as the eastern US, Europe, China, the Amazon basin and central Africa (Figs. S6 and S7 in the Supplement). Driven by anthropogenic pollution aerosols, total radiation decreases by −15 to −30 W m^{-2} (−3 to −15 %), direct radiation decreases by −20 to −50 W m^{-2} (−25 to −80 %) and diffuse radiation increases by +10–25 W m^{-2} (+6–22 %), with largest signals over the eastern US (+15–20 W m^{-2}; +10–14 %) and central Africa (> 25 W m^{-2}; > 14 %).

In summation, anthropogenic pollution aerosols drive an overall SSR (direct + diffuse) global decline of ∼ 5 W m^{-2}. In the literature, estimates for the overall SSR decline during the “global dimming” (period 1950–1980) range from 3 to 9 W m^{-2} (Wild, 2012). In percentage, anthropogenic pollution aerosols drive an overall SSR global

ACPD
15, 25433–25475, 2015

decline of 8.7 %. Regionally, on both annual and seasonal average, North America, Europe, East Asia, the Amazon basin and central Africa are highly affected by aerosol-induced changes in surface solar radiation. The eastern US shows the largest increase in diffuse radiation among industrialized regions. Europe and China undergo a strong reduction in total and direct radiation mainly due to non-biomass burning sources. Both Mercado et al. (2009) and Chen and Zhuang (2014) simulated a consistent increase in diffuse solar radiation in East Asia; Mercado et al. (2013) estimated a increase in diffuse fraction by 25–30 % over East Asia and Europe during the "global dimming" period. Due to biomass burning aerosols, the Amazon basin and central Africa record comparable decrease in total and direct radiation; however, the Amazon basin experiences a weaker increase in diffuse radiation compared to central Africa. Over the Amazon basin, Chen and Zhuang (2014) simulated an aerosol-driven decrease in diffuse radiation; the authors ascribed this behavior to both (a) aerosol-driven decrease in total radiation (less solar radiation to be scattered above, and subsequently under, clouds) and (b) high cloud fractions over the Amazon basin (cloud scattering effectively limits aerosol light scattering).

3.2.2 Surface temperature and relative humidity

Compared to the global effect of pollution aerosols on surface solar radiation, in the short-term pollution aerosols affect surface atmospheric temperature over a few regions: Europe, part of Middle-East, central Africa, the Amazon Basin (Fig. 5a–c). Biomass burning aerosols reduce annual average SAT by −0.6 to −1 K (−0.2 to −0.3 %) in the Amazon basin; a weaker, but similar signal is observed over central Africa (Fig. 5b). Concomitant to a cooling in the Amazon basin, surface RH increases by +1.5–3 % (Fig. 5e), with a maximum rise at the peak of the dry-fire season (+4–6 % during boreal summer, Figs. S11 and S12 in the Supplement). On annual average, anthropogenic pollution aerosols drive a rise in surface RH by +1–1.5 % in the eastern North-America experiences. In this region, during the growing season (boreal sum-

ACPD
15, 25433–25475, 2015

mer), SAT decreases by −1 to −1.5 K (−0.4 to −0.6 %) and surface RH increases by +4–6 % (Figs. S11 and S12 in the Supplement).

The evolution of surface temperature and relative humidity are tightly connected through vegetation. Cooler surface temperatures reduce canopy temperatures and favor an increase in canopy conductance and RH, via evapotranspiration; hence, aerosol-driven cooling may lastly induce a change in the water cycle. However, in our experiment we do not observe robust changes in precipitation nor in total cloud cover. Reduction in surface temperature may favor plant productivity, if temperatures are above the temperature optimum for photosynthesis (25 °C). The role of surface temperature for plant photosynthesis might be important in tropical regions where carbonaceous aerosols from biomass burning efficiently absorb incoming solar radiation and induce a cooling at the surface. Elsewhere, change in the quantity and quality of surface solar radiation may play the main role in affecting plant photosynthesis. In the following section, we analyze aerosol-driven changes in land carbon fluxes and we link them to changes in SSR and SAT.

3.3 Global sensitivity of GPP and isoprene emission to aerosol pollution

The global annual average GPP flux and isoprene emissions for each simulation are reported in Table 2. Across all simulations global annual GPP and isoprene emission are consistent with actual estimates of the present-day carbon cycle budget (GPP: $123 \pm 8\,\mathrm{Pg\,C\,yr^{-1}}$, Beer et al., 2010; isoprene: $400–700\,\mathrm{Tg\,C\,yr^{-1}}$, Guenther et al., 2006).

Global GPP and isoprene emission are not sensitive to pollution aerosols (Table 2). Global GPP is reduced by up to −2.0 % ($-2.4\,\mathrm{Pg\,C\,yr^{-1}}$) at most for SimNOant. Global isoprene emission increases by up to +2.0 % ($+6.9\,\mathrm{Tg\,C\,yr^{-1}}$) for SimNOant. Removal of biomass burning emissions has almost zero effects on global GPP and isoprene emission.

Under removal of all anthropogenic pollution aerosols, we observe a change in global GPP that is half the value obtained by Chen and Zhuang (2014) ($4.9\,\mathrm{Pg\,C\,yr^{-1}}$). How-

ACPD
15, 25433–25475, 2015

ever, Chen and Zhuang (2014) removed all atmospheric aerosols and simulated a decrease in total radiation of $-21.9\,W\,m^{-2}$, which is four times the reduction we simulated in total radiation ($-5.2\,W\,m^{-2}$). Furthermore, they applied transient atmospheric CO_2 and prognostic LAI; hence, aerosol-induced changes in environmental parameters (e.g., light, temperature, CO_2 concentration) affect plant productivity as well plant phenology. In contrast with Mercado et al. (2009), we do not ascertain a significant change in global GPP due to removal of pollution aerosols.

3.3.1 Regional sensitivity of GPP to aerosol pollution

Anthropogenic aerosol pollution drives regional increases in annual average plant productivity (Fig. 6). The strongest increases in GPP occur in eastern North America and Europe ($+0.2$–$0.4\,g\,C\,m^{-2}\,day^{-1}$; +8–12 %, Fig. 6a). Biomass burning aerosols drive increases in GPP of $+0.2$–$0.4\,g\,C\,m^{-2}\,day^{-1}$ (+2–5 %) in the Amazon basin, central Africa and eastern Europe (Fig. 6b). Industrial pollution aerosols increase GPP by $+0.05$–$0.2\,g\,C\,m^{-2}\,day^{-1}$ (+2–5 %) in the eastern US (Great Lakes region), Europe and Asia (China and South-Eastern Asia) (Fig. 6c).

During boreal summer, anthropogenic aerosol pollution increases GPP in North America and Europe by up to +12 % (> 0.6–$0.8\,g\,C\,m^{-2}\,day^{-1}$, Fig. 7). Comparison between SimCTRL-SimNOant and SimCTRL-SimNOind indicates that pollution emissions from non-biomass burning sources (industry, power generation, road vehicles) drive these increases (Fig. 7a vs. Fig. 7c). In the dry-fire season (boreal summer and fall; here, only summer is shown), biomass burning aerosols increase GPP by $+0.05$–$0.4\,g\,C\,m^{-2}\,day^{-1}$ (+2–5 %) in eastern Europe (boreal forests), and by $+0.4$–$0.6\,g\,C\,m^{-2}\,day^{-1}$ (+5–8 %) in the Amazon basin (Fig. 7b).

Pollution aerosols have largest impacts on GPP for PFTs with complex canopy architectures such as deciduous broadleaf and evergreen needleleaf forests and rainforests, in agreement with observational studies (e.g., Niyogi et al., 2004; Alton et al., 2007; Cirino et al., 2014).

ACPD
15, 25433–25475, 2015

Anthropogenic pollution aerosols, mainly from non-biomass burning sources, enhance plant productivity in industrialized regions such as eastern North America, Europe and China. These industrialized regions undergo considerable changes in surface solar radiation due to anthropogenic pollution aerosols (Fig. 4). The eastern US records the largest increase in diffuse radiation that likely induces a reduction in SAT and, consequently, in canopy temperature. On the contrary, Europe and China experience a strong reduction in total and direct radiation. Simulated enhancement in plant productivity in the cited regions agrees with both observational and modeling studies (e.g., Niyogi et al., 2004; Steiner and Chameides, 2005; Knohl and Baldocchi, 2008; Matsui et al., 2008). In eastern North America, Europe and China, Mercado et al. (2009) simulated a substantial land carbon uptake due to diffuse-fraction contribution between 1950 and 1980 ("global dimming" for SSR, Wild et al., 2009). However, the authors observed changes in land carbon uptake due to diffuse-fraction contribution that are one order of magnitude smaller than our results (+0.03–0.07 $g C m^{-2} day^{-1}$; see Fig. 2d in Mercado et al., 2009); moreover, diffuse fraction seems to be unchanged over the eastern North America (see Fig. 2c in Mercado et al., 2009). Chen and Zhuang (2014) simulated positive aerosol effects on GPP in North America, Europe, central Africa and South and East Asia; however, they recorded the largest increase in GPP in central Africa and Asia (+0.8–1 $g C m^{-2} day^{-1}$; see Fig. 4a in Chen and Zhuang, 2014).

Biomass burning aerosols enhance plant productivity in the Amazon basin and central Africa. These biomass burning regions observe a comparable decrease in total and direct radiation; however, the Amazon basin experiences a weaker increase in diffuse radiation, but a larger cooling compared to central Africa (Fig. 5). In the Amazon basin, previous studies observed enhancement in CO_2 uptake at ecosystem scale during biomass burning season; these observational studies mainly attributed rise in CO_2 uptake to the increase in diffuse light, although significant changes in surface temperature and humidity were measured (e.g., Oliveira et al., 2007; Doughty et al., 2010; Cirino et al., 2014). Notably, aerosol-induced reduction in surface temperature directly affects leaf temperature and might be important for sunlit leaves (Doughty et al., 2010).

ACPD
15, 25433–25475, 2015

Based on a modeling study, Rap et al. (2015) estimated that BBAs enhance GPP by 0.7–1.6 %, under an increase in diffuse radiation by 3.4–6.8 %. These perturbations are weaker than our results; Rap et al. (2015) stated that their results might be conservative because they do not accounted for aerosol-induced reduction in leaf temperature. In contrast with our results, Chen and Zhuang (2014) simulated a negative aerosol effects on GPP in the Amazon basin. The authors ascribed this reduction in GPP to the high cloud fraction and water vapor concentration over the region that both reduce incoming solar radiation and, consequently, aerosol light-scattering. Due to the large cooling and the role of high cloud fraction and water vapor concentration in limiting diffuse radiation in the Amazon basin, we hypothesize that the aerosol-induced cooling is the main driver of GPP enhancement.

Anthropogenic aerosol pollution significantly enhances plant productivity at a regional scale. The aerosol-driven enhancement in GPP seems to result from three different mechanisms: (1) light scattering, which partly reduces canopy temperature (eastern US), (2) reduction in direct radiation (Europe and China), and (3) cooling (the Amazon basin).

3.3.2 Regional sensitivity of plant isoprene emission to aerosol pollution

Compared to GPP, isoprene emission has an opposite and uneven sensitivity to pollution aerosols (Fig. 8). Anthropogenic aerosol pollution drives a decrease in annual average isoprene emission of −0.5 to −1 mg C m^{-2} day^{-1} (−2 to −12 %) over Europe and China (Fig. 8a). Pollution emissions from non-biomass burning sources are the main drivers, as comparison between SimCTRL-SimNObb and SimCTRL-SimNOind indicates (Fig. 8b vs. Fig. 8c). During boreal summer, pollution aerosols do not affect isoprene emission (Fig. 9).

On both annual and seasonal average, Europe and China have a lower isoprene flux compared to the main isoprene source regions (the Amazon basin, central Africa and the eastern US). Under aerosol pollution, Europe and China record a larger decrease in direct radiation (< −40 %), and a weaker increase in diffuse radiation (+8–10 %),

ACPD
15, 25433–25475, 2015

compared to high-isoprene regions such as the eastern US and central Africa ($\Delta_{\%}$ Direct Radiation from −40 to −30 %; $\Delta_{\%}$ Diffuse Radiation > +10 %) (Fig. 4a–c). Over Europe and China aerosol-driven reduction in direct light is not adequately sustained by an increase in diffuse radiation and may considerably limit isoprene emission, due to a reduced light supply (reduced J_e). Recently, Stavrakou et al. (2014) analyzed the interannual variability in isoprene source in Asia for the period 1979–2012 by applying sensitivity simulations, in-situ measurements and formaldehyde (HCOC used as VOC proxy) spaceborne observations. Compared to a well-established inventory of biogenic emissions, the authors found that isoprene source in Asia is a factor of 2 lower. The decreasing trend in isoprene source is confirmed by satellite-derived isoprene emission estimates: inferred isoprene fluxes decrease by 2.1 Tg over China between 2007 and 2012 (Stavrakou et al., 2014). In China, we find that lower SSR caused by the aerosol loading drives a decrease of ∼ 10 % in the isoprene source, on an annual average. Over Europe and China, the sensitivity of isoprene emission to aerosol pollution diverges from GPP sensitivity. We discuss below this divergent regional response of GPP and isoprene to aerosol pollution.

3.3.3 Divergent regional sensitivity of GPP and isoprene emission to aerosol pollution

The divergent response over Europe and China (i.e., aerosol-driven GPP increase and concomitant isoprene decrease) suggests a "decoupling" between the modeled processes of photosynthesis and isoprene emission over these regions. In Europe and China, we posit that aerosol-induced reduction in direct radiation drives isoprene decreases and concomitant GPP increases. In the model, the rate of net CO_2 uptake results from the minimum of three competing processes: supply of the Rubisco enzyme (J_c); supply of light (J_e) and supply of nutrients (J_s). As theoretical and observational studies have demonstrated, the aerosol effect on plant photosynthesis strongly depends on the canopy separation into sunlit and shaded leaves. These two parts of the canopy have different responses to the change in light partitioning driven by aerosols

ACPD
15, 25433–25475, 2015

(Knohl and Baldocchi, 2008). Under low PAR, both shaded and sunlit leaves are in a light-limited environment (J_e controls the photosynthetic rate). Under high PAR, sunlit leaves are light-saturated and in a Rubisco-limited environment (J_c controls the photosynthetic rate), while shaded leaves are in a light-limited environment (J_e). Hence, sunlit canopy photosynthesis depends on both direct and diffuse light, and on both the J_c and J_e photosynthesis rate; while shaded canopy photosynthesis is directly influenced by diffuse light and depends on the J_e photosynthesis rate. The aerosol light-scattering directly influences J_e, hence it mainly affects shaded leaves (Matsui et al., 2008; Chen and Zhuang, 2014).

At the same time, in the model, isoprene emission depends on light supply (J_e), hence isoprene emission continues to rise under increasing PAR, even when photosynthesis is light-saturated (in a Rubisco-limited environment) (Morfopoulos et al., 2013). This response was observed at the ecosystem scale and showed an important dependence on both light quantity and temperature (Sharkey and Loreto, 1993). At 20 °C and at any photon flux, the authors recorded nearly no isoprene emission; at 30 °C isoprene emission increased with photon flux up to 1600 µmol m^{-2} s^{-1}, while photosynthesis was already saturated; at 40 °C, isoprene emission maximized at 1000 µmol m^{-2} s^{-1}, afterwards it decreased when the photon flux raised to 1600 µmol m^{-2} s^{-1}.

In the model, isoprene emission in the Amazon basin is not sensitive to pollution aerosols. Over this region, absorbing and scattering aerosols from biomass burning significantly reduce direct radiation and surface temperature, with a smaller increase in diffuse radiation compared to central Africa. Isoprene synthase has a larger temperature optimum (35 °C) compared to photosynthesis (25 °C), hence isoprene emission will decrease under cooling conditions. Since in the Amazon basin isoprene emission does not respond to the aerosol-driven decrease in direct radiation, implying offsetting thermal and radiative responses, we deduce that aerosol-driven cooling in the Amazon basin plays a role in increasing the plant productivity there on an annual and seasonal scale.

ACPD
15, 25433–25475, 2015

We posit that the aerosol-induced rise in diffuse radiation (the diffuse fertilization effect) drives enhancement in plant productivity in the eastern US This region experiences one of the largest increase in diffuse light that may enhance GPP via the increase of J_e photosynthesis rate in shaded leaves. The concomitant cooling observed in the eastern US may limit the sensitivity of isoprene emission to an increase in the supply of light.

To conclude, anthropogenic aerosols affect GPP and isoprene emissions via three mechanisms: (1) light scattering, (2) cooling, and (3) reduction in direct radiation. We suggest that the dominant aerosol-driven mechanism that influences land carbon fluxes varies across regions: (1) light scattering, and concomitant cooling, dominates in the eastern US; (2) cooling dominates in the Amazon basin; and (3) reduction in direct radiation dominates in Europe and China.

4 Discussion and conclusions

Aerosol-induced effects on land carbon fluxes (GPP and isoprene emission) were investigated using a coupled vegetation–chemistry–climate model. By performing sensitivity experiments, we isolated the role of pollution aerosol sources (all anthropogenic, biomass burning and non-biomass burning).

We acknowledge three main limitations in our study. Firstly, we tackled the direct aerosol effects only and did not consider 1st and 2nd indirect effects of aerosols. Hence, we are partly missing the impact of aerosol–cloud interactions on the land carbon fluxes. Secondly, we used the fixed SST-technique, hence we accounted only for rapid adjustments of land surface climate to aerosol radiation perturbation. Thirdly, we prescribed LAI, hence plant phenology does not respond to the changes in aerosol pollution. We are likely underestimating the magnitude of aerosol-induced effects on plant productivity by not including these feedbacks.

Despite these limitations, our results suggest that global-scale land carbon fluxes (GPP and isoprene emission) are not sensitive to the direct effects of pollution aerosols,

ACPD
15, 25433–25475, 2015

even under a robust overall SSR (direct + diffuse) global change (∼ 9 %). We found a significant, but divergent, sensitivity of GPP and isoprene emission to pollution aerosols at the regional scale, in locations where complex canopies dominate. In eastern North America and Europe, anthropogenic pollution aerosols (mainly from non-biomass burning sources) enhance GPP by +8–12 % on an annual average, with a stronger increase during the growing season (> 12 %). In the Amazon basin and central Africa, biomass burning aerosols increase GPP by +2–5 % on an annual average (+5–8 % at the peak of the dry-fire season in the Amazon basin). In Europe and China, anthropogenic pollution aerosols (mainly from non-biomass burning sources) drive a decrease in isoprene emission of −2 to −12 % on annual average. This study highlights the importance of accounting for both aerosol-induced radiative and thermal effects on plant productivity (Steiner and Chameides, 2005). Our model results imply that a further reduction of anthropogenic pollution aerosols over Europe may trigger an enhancement in isoprene emission, with consequences on ozone production/destruction (depending on NO_x levels), methane lifetime and secondary aerosols (through BSOA production). In future research, we will (1) assess co-impacts of aerosol indirect effects, (2) apply a fully coupled ocean-atmosphere global climate model (GCM) to quantify the long-term aerosol climate effects (e.g., Koch et al., 2009); (3) apply a full land carbon cycle model with dynamic LAI and tree growth, and respiration responses (Yue and Unger, 2015).

The Supplement related to this article is available online at doi:10.5194/acpd-15-25433-2015-supplement.

Author contributions. S. Strada and N. Unger designed the experiments. S. Strada performed the simulations. S. Strada and N. Unger prepared the manuscript.

Acknowledgements. This project was supported in part by the facilities and staff of the Yale University Faculty of Arts and Sciences High Performance Computing Center.

ACPD
15, 25433–25475, 2015

References

Alton, P. B., North, P. R., and Los, S. O.: The impact of diffuse sunlight on canopy light-use efficiency, gross photosynthetic product and net ecosystem exchange in three forest biomes, Global Change Biol., 13, 776–787, 2007. 25449

Arneth, A., Monson, R. K., Schurgers, G., Niinemets, Ü., and Palmer, P. I.: Why are estimates of global terrestrial isoprene emissions so similar (and why is this not so for monoterpenes)?, Atmos. Chem. Phys., 8, 4605–4620, doi:10.5194/acp-8-4605-2008, 2008. 25442

Artaxo, P., Rizzo, L. V., Brito, J. F., Barbosa, H. M. J., Arana, A., Sena, E. T., Cirino, G. G., Bastos, W., Martin, S. T., and Andreae, M. O.: Atmospheric aerosols in Amazonia and land use change: from natural biogenic to biomass burning conditions, Faraday Discuss., 165, 203–235, doi:, 2013. 25436

Bauer, S. E., Koch, D., Unger, N., Metzger, S. M., Shindell, D. T., and Streets, D. G.: Nitrate aerosols today and in 2030: a global simulation including aerosols and tropospheric ozone, Atmos. Chem. Phys., 7, 5043–5059, doi:10.5194/acp-7-5043-2007, 2007. 25439

Beer, C., Reichstein, M., Tomelleri, E., Ciais, P., Jung, M., Carvalhais, N., Rödenbeck, C., Arain, M. A., Baldocchi, D., Bonan, G. B., Bondeau, A., Cescatti, A., Lasslop, G., Lindroth, A., Lomas, M., Luyssaert, S., Margolis, H., Oleson, K. W., Roupsard, O., Veenendaal, E., Viovy, N., Williams, C., Woodward, F. I., and Papale, D.: Terrestrial gross carbon dioxide uptake: global distribution and covariation with climate, Science, 329, 834–838, 2010. 25434, 25438, 25442, 25448

Bell, N., Koch, D., and Shindell, D.: Impacts of chemistry-aerosol coupling on tropospheric ozone and sulfate simulations in a general circulation model, J. Geophys. Res.-Atmos., 110, D14, doi:10.1029/2004JD005538, 2005. 25439

Bian, H., Chin, M., Kawa, S. R., Yu, H., Diehl, T., and Kucsera, T.: Multiscale carbon monoxide and aerosol correlations from satellite measurements and the GOCART model: implication for emissions and atmospheric evolution, J. Geophys. Res.-Atmos., 115, D07302, doi:10.1029/2009JD012781, 2010. 25443

Bonan, G. B., Lawrence, P. J., Oleson, K. W., Levis, S., Jung, M., Reichstein, M., Lawrence, D., and Swenson, S. C.: Improving canopy processes in the Community Land Model version 4 (CLM4) using global flux fields empirically inferred from FLUXNET data, J. Geophys. Res.-Biogeo., 116, G2, doi:10.1029/2010JG001593, 2011. 25438

ACPD
15, 25433–25475, 2015

Boucher, O., Randall, D., Artaxo, P., Bretherton, C., Feingold, G., Forster, P., Kerminen, V.-M., Kondo, Y., Liao, H., Lohmann, U., Rasch, P., Satheesh, S. K., Sherwood, S., Stevens, B., and Zhang, X. Y.: Clouds and Aerosols, in: Climate Change 2013: The Physical Science Basis. Contribution of Working Group I to the Fifth Assessment Report of the Intergovernmental Panel on Climate Change, Cambridge University Press, Cambridge, UK and New York, NY, USA, 571–656, 2013. 25438, 25442

Carlton, A. G., Pinder, R. W., Bhave, P. V., and Pouliot, G. A.: To what extent can biogenic SOA be controlled?, Environ. Sci. Technol., 44, 3376–3380, 2010. 25446

Chen, M. and Zhuang, Q.: Evaluating aerosol direct radiative effects on global terrestrial ecosystem carbon dynamics from 2003 to 2010, Tellus B, 66, 21808, doi:, 2014. 25437, 25447, 25448, 25449, 25450, 25451, 25453

Cheng, S. J., Bohrer, G., Steiner, A. L., Hollinger, D. Y., Suyker, A., Phillips, P. R., and Nadelhoffer, K. J.: Variations in the influence of diffuse light on gross primary productivity in temperate ecosystems, Agr. Forest Meteorol., 201, 98–110, 2015. 25436

Cirino, G. G., Souza, R. A. F., Adams, D. K., and Artaxo, P.: The effect of atmospheric aerosol particles and clouds on net ecosystem exchange in the Amazon, Atmos. Chem. Phys., 14, 6523–6543, doi:10.5194/acp-14-6523-2014, 2014. 25436, 25449, 25450

Collatz, G. J., Ball, J. T., Grivet, C., and Berry, J. A.: Physiological and environmental regulation of stomatal conductance, photosynthesis and transpiration: a model that includes a laminar boundary layer, Agr. Forest Meteorol., 54, 107–136, 1991. 25440

Doughty, C. E., Flanner, M. G., and Goulden, M. L.: Effect of smoke on subcanopy shaded light, canopy temperature, and carbon dioxide uptake in an Amazon rainforest, Global Biogeochem. Cy., 24, GB3015, doi:10.1029/2009GB003670, 2010. 25450

Farquhar, G. D., von Caemmerer, S. V., and Berry, J. A.: A biochemical model of photosynthetic CO_2 assimilation in leaves of C_3 species, Planta, 149, 78–90, 1980. 25440

Ford, B. and Heald, C. L.: Aerosol loading in the Southeastern United States: reconciling surface and satellite observations, Atmos. Chem. Phys., 13, 9269–9283, doi:10.5194/acp-13-9269-2013, 2013. 25446

Friend, A. D. and Kiang, N. Y.: Land surface model development for the GISS GCM: effects of improved canopy physiology on simulated climate, J. Climate, 18, 2883–2902, 2005. 25440

Gu, L., Baldocchi, D., Verma, S. B., Black, T., Vesala, T., Falge, E. M., and Dowty, P. R.: Advantages of diffuse radiation for terrestrial ecosystem productivity, J. Geophys. Res.-Atmos., 107, D6, doi:10.1029/2001JD001242, 2002. 25436

ACPD
15, 25433–25475, 2015

Gu, L., Baldocchi, D. D., Wofsy, S. C., Munger, J. W., Michalsky, J. J., Urbanski, S. P., and Boden, T. A.: Response of a deciduous forest to the Mount Pinatubo eruption: enhanced photosynthesis, Science, 299, 2035–2038, 2003. 25435, 25436

Guenther, A., Karl, T., Harley, P., Wiedinmyer, C., Palmer, P. I., and Geron, C.: Estimates of global terrestrial isoprene emissions using MEGAN (Model of Emissions of Gases and Aerosols from Nature), Atmos. Chem. Phys., 6, 3181–3210, doi:10.5194/acp-6-3181-2006, 2006. 25442, 25448

Hsu, N. C., Tsay, S.-C., King, M., and Herman, J. R.: Aerosol properties over bright-reflecting source regions, IEEE T. Geosci. Remote, 42, 557–569, doi:10.5194/amt-7-1791-2014, 2004. 25443

Jones, C. D. and Cox, P. M.: Modeling the volcanic signal in the atmospheric CO_2 record, Global Biogeochem. Cy., 15, 453–465, 2001. 25435

Jung, M., Reichstein, M., Margolis, H. A., Cescatti, A., Richardson, A. D., Arain, M. A., Arneth, A., Bernhofer, C., Bonal, D., Chen, J., Gianelle, D., Gobron, N., Kiely, G., Kutsch, W., Lasslop, G., Law, B. E., Lindroth, A., Merbold, L., Montagnani, L., Moors, E. J., Papale, D., Sottocornola, M., Vaccari, F., and Williams, C.: Global patterns of land-atmosphere fluxes of carbon dioxide, latent heat, and sensible heat derived from eddy covariance, satellite, and meteorological observations, J. Geophys. Res.-Biogeo., 116, G3, doi:10.1029/2010JG001566, 2011. 25438

Kanniah, K. D., Beringer, J., North, P., and Hutley, L.: Control of atmospheric particles on diffuse radiation and terrestrial plant productivity: a review, Prog. Phys. Geogr., 36, 209–237, 2012. 25436

Keeling, C. D., Whorf, T. P., Wahlen, M., and Plicht, J. V. D.: Interannual extremes in the rate of rise of atmospheric carbon dioxide since 1980, Nature, 375, 666–670, 1995. 25435

Knohl, A. and Baldocchi, D. D.: Effects of diffuse radiation on canopy gas exchange processes in a forest ecosystem, J. Geophys. Res.-Biogeo., 113, G2, doi:10.1029/2007JG000663, 2008. 25450, 25453

Koch, D. and Del Genio, A. D.: Black carbon semi-direct effects on cloud cover: review and synthesis, Atmos. Chem. Phys., 10, 7685–7696, doi:10.5194/acp-10-7685-2010, 2010. 25439

Koch, D. and Hansen, J.: Distant origins of Arctic black carbon: a Goddard Institute for Space Studies ModelE experiment, J. Geophys. Res., 110, 7685–7696, doi:10.1029/2004JD005296, 2005. 25439

ACPD
15, 25433–25475, 2015

Koch, D., Schmidt, G. A., and Field, C. V.: Sulfur, sea salt, and radionuclide aerosols in GISS ModelE, J. Geophys. Res., 111, doi:10.1029/2004JD005550, 2006. 25439
Koch, D., Menon, S., Del Genio, A., Ruedy, R., Alienov, I., and Schmidt, G. A.: Distinguishing aerosol impacts on climate over the past century, J. Climate, 22, 2659–2677, doi:10.1175/2008JCLI2573.1, 2009. 25455
Laffineur, Q., Aubinet, M., Schoon, N., Amelynck, C., Müller, J.-F., Dewulf, J., Steppe, K., and Heinesch, B.: Impact of diffuse light on isoprene and monoterpene emissions from a mixed temperate forest, Atmos. Environ., 74, 385–392, 2013. 25436
Lamarque, J.-F., Bond, T. C., Eyring, V., Granier, C., Heil, A., Klimont, Z., Lee, D., Liousse, C., Mieville, A., Owen, B., Schultz, M. G., Shindell, D., Smith, S. J., Stehfest, E., Van Aardenne, J., Cooper, O. R., Kainuma, M., Mahowald, N., McConnell, J. R., Naik, V., Riahi, K., and van Vuuren, D. P.: Historical (1850–2000) gridded anthropogenic and biomass burning emissions of reactive gases and aerosols: methodology and application, Atmos. Chem. Phys., 10, 7017–7039, doi:10.5194/acp-10-7017-2010, 2010. 25441
Levy, R. C., Remer, L. A., Kleidman, R. G., Mattoo, S., Ichoku, C., Kahn, R., and Eck, T. F.: Global evaluation of the Collection 5 MODIS dark-target aerosol products over land, Atmos. Chem. Phys., 10, 10399–10420, doi:10.5194/acp-10-10399-2010, 2010. 25443
Matsui, T., Beltrán-Przekurat, A., Niyogi, D., Pielke, R. A., and Coughenour, M.: Aerosol light scattering effect on terrestrial plant productivity and energy fluxes over the eastern United States, J. Geophys. Res.-Atmos., 113, D14, doi:10.1029/2007JD009658, 2008. 25436, 25450, 25453
Mercado, L. M., Bellouin, N., Sitch, S., Boucher, O., Huntingford, C., Wild, M., and Cox, P. M.: Impact of changes in diffuse radiation on the global land carbon sink, Nature, 458, 1014–1017, 2009. 25437, 25447, 25449, 25450
Miller, R., Cakmur, R. V., Perlwitz, J. P., Geogdzhayev, I. V., Ginoux, P., Kohfeld, K. E., Koch, D., Prigent, C., Ruedy, R., Schmidt, G. A., and Tegen, I.: Mineral dust aerosols in the NASA Goddard Institute for Space Sciences ModelE atmospheric general circulation model, J. Geophys. Res., 111, 474–487, doi:10.1029/2005JD005796, 2006. 25439
Molineaux, B. and Ineichen, P.: Impact of Pinatubo aerosols on the seasonal trends of global, direct and diffuse irradiance in two northern mid-latitude sites, Sol. Energy, 58, 91–101, doi:10.1016/0038-092X(96)00051-5, 1996. 25435
Morfopoulos, C., Prentice, I. C., Keenan, T. F., Friedlingstein, P., Medlyn, B. E., Peñuelas, J., and Possell, M.: A unifying conceptual model for the environmental responses of isoprene

ACPD
15, 25433–25475, 2015

emissions from plants, Ann. Bot.-London, 112, 1223–1238, doi:10.1093/aob/mct206, 2013. 25453

Myhre, G., Samset, B. H., Schulz, M., Balkanski, Y., Bauer, S., Berntsen, T. K., Bian, H., Bellouin, N., Chin, M., Diehl, T., Easter, R. C., Feichter, J., Ghan, S. J., Hauglustaine, D., Iversen, T., Kinne, S., Kirkevåg, A., Lamarque, J.-F., Lin, G., Liu, X., Lund, M. T., Luo, G., Ma, X., van Noije, T., Penner, J. E., Rasch, P. J., Ruiz, A., Seland, Ø., Skeie, R. B., Stier, P., Takemura, T., Tsigaridis, K., Wang, P., Wang, Z., Xu, L., Yu, H., Yu, F., Yoon, J.-H., Zhang, K., Zhang, H., and Zhou, C.: Radiative forcing of the direct aerosol effect from AeroCom Phase II simulations, Atmos. Chem. Phys., 13, 1853–1877, doi:10.5194/acp-13-1853-2013, 2013a. 25438, 25439

Myhre, G., Shindell, D., Bréon, F.-M., Collins, W., Fuglestvedt, J., Huang, J., Koch, D., Lamarque, J.-F., Lee, D., Mendoza, B., Nakajima, T., Robock, A., Stephens, G., Takemura, T., and Zhang, H.: Anthropogenic and natural radiative forcing, in: Climate Change 2013: The Physical Science Basis. Contribution of Working Group I to the Fifth Assessment Report of the Intergovernmental Panel on Climate Change, Cambridge University Press, Cambridge, UK and New York, NY, USA, 659–740, doi:10.1017/CBO9781107415324.018, 2013b. 25438, 25442

Niyogi, D., Chang, H.-I., Saxena, V. K., Holt, T., Alapaty, K., Booker, F., Chen, F., Davis, K. J., Holben, B., Matsui, T., Meyers, T., Oechel, W. C., Pielke, R. A., Wells, R., Wilson, K., and Xue, Y.: Direct observations of the effects of aerosol loading on net ecosystem CO_2 exchanges over different landscapes, Geophys. Res Lett., 31, 20, doi:10.1029/2004GL020915, 2004. 25436, 25449, 25450

Oliveira, P. H. F., Artaxo, P., Pires, C., De Lucca, S., Procópio, A., Holben, B., Schafer, J., Cardoso, L. F., Wofsy, S. C., and Rocha, H. R.: The effects of biomass burning aerosols and clouds on the CO_2 flux in Amazonia, Tellus B, 59, 338–349, 2007. 25436, 25450

Pacifico, F., Harrison, S. P., Jones, C. D., and Sitch, S.: Isoprene emissions and climate, Atmos. Environ., 43, 6121–6135, doi:10.1016/j.atmosenv.2009.09.002, 2009. 25435

Ramanathan, V., Crutzen, P., Kiehl, J., and Rosenfeld, D.: Aerosols, climate, and the hydrological cycle, Science, 294, 2119–2124, 2001. 25435

Rap, A., Spracklen, D. V., Mercado, L., Reddington, C. L., Haywood, J. M., Ellis, R. J., Phillips, O. L., Artaxo, P., Bonal, D., Coupe, N. R., and Butt, N.: Fires increase Amazon forest productivity through increases in diffuse radiation, Geophys. Res. Lett., 42, 4654–4662, doi:10.1002/2015GL063719, 2015. 25436, 25437, 25451

ACPD
15, 25433–25475, 2015

Rayner, N., Brohan, P., Parker, D., Folland, C., Kennedy, J., Vanicek, M., Ansell, T., and Tett, S.: Improved analyses of changes and uncertainties in sea surface temperature measured in situ since the mid-nineteenth century: the HadSST2 dataset, J. Climate, 19, 446–469, 2006. 25441

Rosenfeld, D., Lohmann, U., Raga, G. B., O'Dowd, C. D., Kulmala, M., Fuzzi, S., Reissell, A., and Andreae, M. O.: Flood or drought: how do aerosols affect precipitation?, Science, 321, 1309–1313, 2008. 25435

Rosenzweig, C. and Abramopoulos, F.: Land-surface model development for the GISS GCM, J. Climate, 10, 2040–2054, doi:10.1175/1520-0442(1997)010<2040:LSMDFT>2.0.CO;2, 1997. 25440

Schmidt, G. A., Ruedy, R., Hansen, J. E., Aleinov, I., Bell, N., Bauer, M., Bauer, S., Cairns, B., Canuto, V., Cheng, Y., Del Genio, A., Faluvegi, G., Friend, A. D., Hall, T. M., Hu, Y., Kelley, M., Kiang, N. Y., Koch, D., Lacis, A. A., Lerner, J., Lo, K. K., Miller, R. L., Nazarenko, L., Oinas, V., Perlwitz, J. P., Perlwitz, J., Rind, D., Romanou, A., Russell, G. L., Sato, M., Shindell, D. T., Stone, P. H., Sun, S., Tausnev, N., Thresher, D., and Yao, M.-S.: Present-day atmospheric simulations using GISS ModelE: comparison to in situ, satellite, and reanalysis data, J. Climate, 19, 153–192, 2006. 25439

Schmidt, G. A., Kelley, M., Nazarenko, L., Ruedy, R., Russell, G. L., Aleinov, I., Bauer, M., Bauer, S. E., Bhat, M. K., Bleck, R., Canuto, V., Chen, Y.-H., Cheng, Y., Clune, T. L., Del Genio, A., de Fainchtein, R., Faluvegi, G., Hansen, J. E., Healy, R. J., Kiang, N. Y., Koch, D., Lacis, A. A., LeGrande, A. N., Lerner, J., Lo, K. K., Matthews, E. E., Menon, S., Miller, R. L., Oinas, V., Oloso, A. O., Perlwitz, J. P., Puma, M. J., Putman, W. M., Rind, D., Romanou, A., Sato, M., Shindell, D. T., Sun, S., Syed, R. A., Tausnev, N., Tsigaridis, K., Unger, N., Voulgarakis, A., Yao, M.-S., and Zhangand, J.: Configuration and assessment of the GISS ModelE2 contributions to the CMIP5 archive, J. Adv. Model. Earth Syst., 6, 141–184, doi:10.1002/2013MS000265, 2014. 25438, 25440

Sharkey, T. D. and Loreto, F.: Water stress, temperature, and light effects on the capacity for isoprene emission and photosynthesis of kudzu leaves, Oecologia, 95, 328–333, 1993. 25453

Shi, Y., Zhang, J., Reid, J. S., Liu, B., and Hyer, E. J.: Critical evaluation of cloud contamination in the MISR aerosol products using MODIS cloud mask products, Atmos. Meas. Tech., 7, 1791–1801, doi:10.5194/amt-7-1791-2014, 2014. 25443

Shindell, D. T., Faluvegi, G., Unger, N., Aguilar, E., Schmidt, G. A., Koch, D. M., Bauer, S. E., and Miller, R. L.: Simulations of preindustrial, present-day, and 2100 conditions in the NASA

ACPD
15, 25433–25475, 2015

GISS composition and climate model G-PUCCINI, Atmos. Chem. Phys., 6, 4427–4459, doi:10.5194/acp-6-4427-2006, 2006. 25439

Shindell, D. T., Pechony, O., Voulgarakis, A., Faluvegi, G., Nazarenko, L., Lamarque, J.-F., Bowman, K., Milly, G., Kovari, B., Ruedy, R., and Schmidt, G. A.: Interactive ozone and methane chemistry in GISS-E2 historical and future climate simulations, Atmos. Chem. Phys., 13, 2653–2689, doi:10.5194/acp-13-2653-2013, 2013a. 25439

Shindell, D. T., Lamarque, J.-F., Schulz, M., Flanner, M., Jiao, C., Chin, M., Young, P. J., Lee, Y. H., Rotstayn, L., Mahowald, N., Milly, G., Faluvegi, G., Balkanski, Y., Collins, W. J., Conley, A. J., Dalsoren, S., Easter, R., Ghan, S., Horowitz, L., Liu, X., Myhre, G., Nagashima, T., Naik, V., Rumbold, S. T., Skeie, R., Sudo, K., Szopa, S., Takemura, T., Voulgarakis, A., Yoon, J.-H., and Lo, F.: Radiative forcing in the ACCMIP historical and future climate simulations, Atmos. Chem. Phys., 13, 2939–2974, doi:10.5194/acp-13-2939-2013, 2013b. 25439

Spitters, C. J. T., Toussaint, H. A. J. M., and Goudriaan, J.: Separating the diffuse and direct component of global radiation and its implications for modeling canopy photosynthesis Part I. Components of incoming radiation, Agr. Forest Meteorol., 38, 217–229, 1986. 25440

Stavrakou, T., Müller, J.-F., Bauwens, M., De Smedt, I., Van Roozendael, M., Guenther, A., Wild, M., and Xia, X.: Isoprene emissions over Asia 1979–2012: impact of climate and land-use changes, Atmos. Chem. Phys., 14, 4587–4605, doi:10.5194/acp-14-4587-2014, 2014. 25452

Steiner, A. L. and Chameides, W. L.: Aerosol-induced thermal effects increase modelled terrestrial photosynthesis and transpiration, Tellus B, 57, 404–411, 2005. 25436, 25450, 25455

Stevenson, D. S., Young, P. J., Naik, V., Lamarque, J.-F., Shindell, D. T., Voulgarakis, A., Skeie, R. B., Dalsoren, S. B., Myhre, G., Berntsen, T. K., Folberth, G. A., Rumbold, S. T., Collins, W. J., MacKenzie, I. A., Doherty, R. M., Zeng, G., van Noije, T. P. C., Strunk, A., Bergmann, D., Cameron-Smith, P., Plummer, D. A., Strode, S. A., Horowitz, L., Lee, Y. H., Szopa, S., Sudo, K., Nagashima, T., Josse, B., Cionni, I., Righi, M., Eyring, V., Conley, A., Bowman, K. W., Wild, O., and Archibald, A.: Tropospheric ozone changes, radiative forcing and attribution to emissions in the Atmospheric Chemistry and Climate Model Intercomparison Project (ACCMIP), Atmos. Chem. Phys., 13, 3063–3085, doi:10.5194/acp-13-3063-2013, 2013. 25439

ACPD
15, 25433–25475, 2015

Streets, D. G., Yan, F., Chin, M., Diehl, T., Mahowald, N., Schultz, M., Wild, M., Wu, Y., and Yu, C.: Anthropogenic and natural contributions to regional trends in aerosol optical depth, 1980–2006, J. Geophys. Res.-Atmos., 114, D10, doi:10.1029/2008JD011624, 2009. 25437

Trenberth, K. E. and Dai, A.: Effects of Mount Pinatubo volcanic eruption on the hydrological cycle as an analog of geoengineering, Geophys. Res. Lett., 34, L15702, doi:10.1029/2007GL030524, 2007. 25435

Tsigaridis, K. and Kanakidou, M.: Secondary organic aerosol importance in the future atmosphere, Atmos. Environ., 41, 4682–4692, 2007. 25439

Unger, N.: Global climate impact of civil aviation for standard and desulfurized jet fuel, Geophys. Res. Lett., 38, 20, doi:10.1029/2011GL049289, 2011. 25439

Unger, N., Harper, K., Zheng, Y., Kiang, N. Y., Aleinov, I., Arneth, A., Schurgers, G., Amelynck, C., Goldstein, A., Guenther, A., Heinesch, B., Hewitt, C. N., Karl, T., Laffineur, Q., Langford, B., McKinney, K. A., Misztal, P., Potosnak, M., Rinne, J., Pressley, S., Schoon, N., and Serça, D.: Photosynthesis-dependent isoprene emission from leaf to planet in a global carbon–chemistry–climate model, Atmos. Chem. Phys. Discuss., 13, 17717–17791, doi:10.5194/acpd-13-17717-2013, 2013. 25435, 25438, 25441

Von Caemmerer, S. V. and Farquhar, G. D.: Some relationships between the biochemistry of photosynthesis and the gas exchange of leaves, Planta, 153, 376–387, 1981. 25440

Wild, M.: Global dimming and brightening: a review, J. Geophys. Res.-Atmos., 114, D10, doi:10.1029/2008JD011470, 2009. 25435, 25437

Wild, M.: Enlightening global dimming and brightening, B. Am. Meteorol. Soc., 93, 27–37, 2012. 25437, 25446

Wild, M., Trüssel, B., Ohmura, A., Long, C. N., König-Langlo, G., Dutton, E. G., and Tsvetkov, A.: Global dimming and brightening: an update beyond 2000, J. Geophys. Res.-Atmos., 114, D10, doi:10.1029/2008JD011382, 2009. 25450

Yuan, W., Liu, S., Yu, G., Bonnefond, J.-M., Chen, J., Davis, K., Desai, A. R., Goldstein, A. H., Gianelle, D., Rossi, F., Suyker, A. E., and Verma, S. B.: Global estimates of evapotranspiration and gross primary production based on MODIS and global meteorology data, Remote Sens. Environ., 114, 1416–1431, 2010. 25442

Yue, X. and Unger, N.: The Yale Interactive terrestrial Biosphere model version 1.0: description, evaluation and implementation into NASA GISS ModelE2, Geosci. Model Dev., 8, 2399–2417, doi:10.5194/gmd-8-2399-2015, 2015. 25455

ACPD
15, 25433–25475, 2015

Zhao, M., Heinsch, F. A., Nemani, R. R., and Running, S. W.: Improvements of the MODIS terrestrial gross and net primary production global data set, Remote Sens. Environ., 95, 164–176, 2005. 25442

ACPD
15, 25433–25475, 2015

Table 1. Global annual average of aerosol column burden (ACB, $mg\,m^{-2}$) and of the effective radiative forcing (ERF) for aerosol–radiation interactions ($W\,m^{-2}$) as simulated by NASA ModelE2-YIBs in the control present-day simulation (20 run years) for, in the order: sulfates, nitrates, organic (OC) and black carbon (BC) from industrial (ind) and biomass burning (bb), and secondary organic aerosols (SOA). Empty cases refer to negligible values (i.e., order of magnitude is: $pg\,m^{-2}$ for ACB; $\mu W\,m^{-2}$ for ERF).

Simulation		SO_4	NO_3	OC_{ind}	OC_{bb}	BC_{ind}	BC_{bb}	SOA
SimCTRL	ACB ($mg\,m^{-2}$)	2.41	5.16	0.48	0.97	0.17	0.09	1.37
	ERF ($W\,m^{-2}$)	−0.76	−0.45	−0.06	−0.11	0.18	0.12	−0.16
SimNOant	ACB ($mg\,m^{-2}$)	1.55	0.69					0.39
	ERF ($W\,m^{-2}$)	−0.45	−0.07					−0.06
SimNObb	ACB ($mg\,m^{-2}$)	2.42	3.54	0.48		0.17		1.14
	ERF ($W\,m^{-2}$)	−0.76	−0.31	−0.06		0.18		−0.13
SimNOind	ACB ($mg\,m^{-2}$)	1.51	1.47		0.82		0.08	0.90
	ERF ($W\,m^{-2}$)	−0.46	−0.14		−0.10		0.10	−0.11

ACPD
15, 25433–25475, 2015

Table 2. Global annual average gross primary productivity (GPP), isoprene emission and shortwave visible (SW VIS) total, direct and diffuse solar radiation as simulated by NASA ModelE2-YIBs in the control and sensitivity present-day simulations (20 run years).

Simulation	GPP	Isoprene	SW VIS Solar Radiation		
			Total	Direct	Diffuse
	($Pg\,C\,yr^{-1}$)	($Tg\,C\,yr^{-1}$)	($W\,m^{-2}$)		
SimCTRL	116.0	402.8	230.9	80.3	150.6
SimNOant	113.6	409.7	236.1	89.3	146.8
SimNObb	114.8	402.9	232.6	83.2	149.4
SimNOind	114.7	407.8	234.7	86.7	148.0

ACPD
15, 25433–25475, 2015

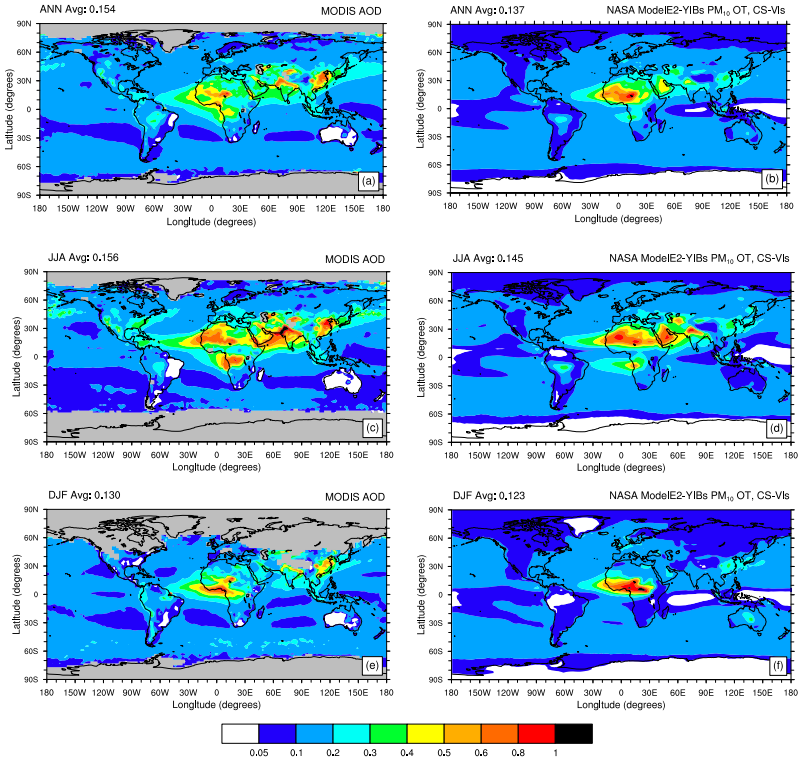

Figure 1. Annual and seasonal average coarse aerosol optical depth (AOD) seen by: **(a, c, e)** the MODIS instrument (at 550 nm; averaged over 2000–2007), and **(b, d, f)** NASA ModelE2-YIBs in the control present-day simulation (20 run years; ~ 2000s). Global mean values are given in the upper left corner of each map. Only boreal summer (JJA) and winter (DJF) seasonal averages are shown. For NASA ModelE2-YIBs, only clear-sky (CS) values in the visible (Vis) range are used to define PM_{10} optical thickness (OT).

ACPD
15, 25433–25475, 2015

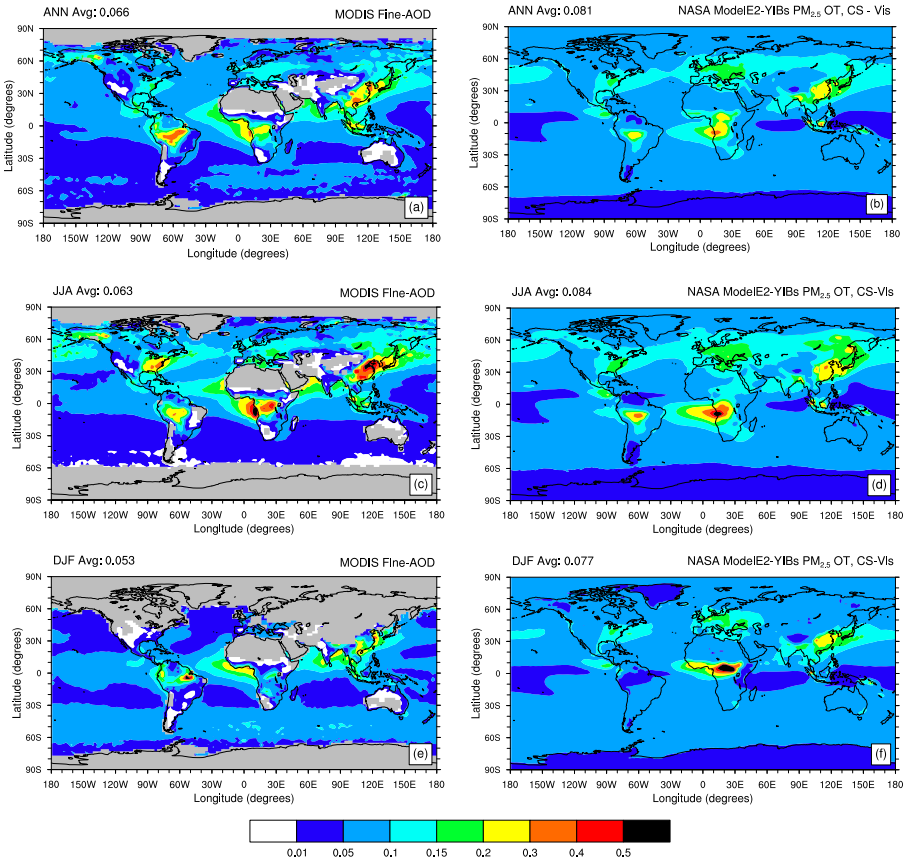

Figure 2. As Fig. 1 for fine-mode aerosol optical depth: **(a, c, e)** MODIS fine-AOD, and **(b, d, f)** model $PM_{2.5}$ OT.

ACPD
15, 25433–25475, 2015

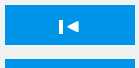

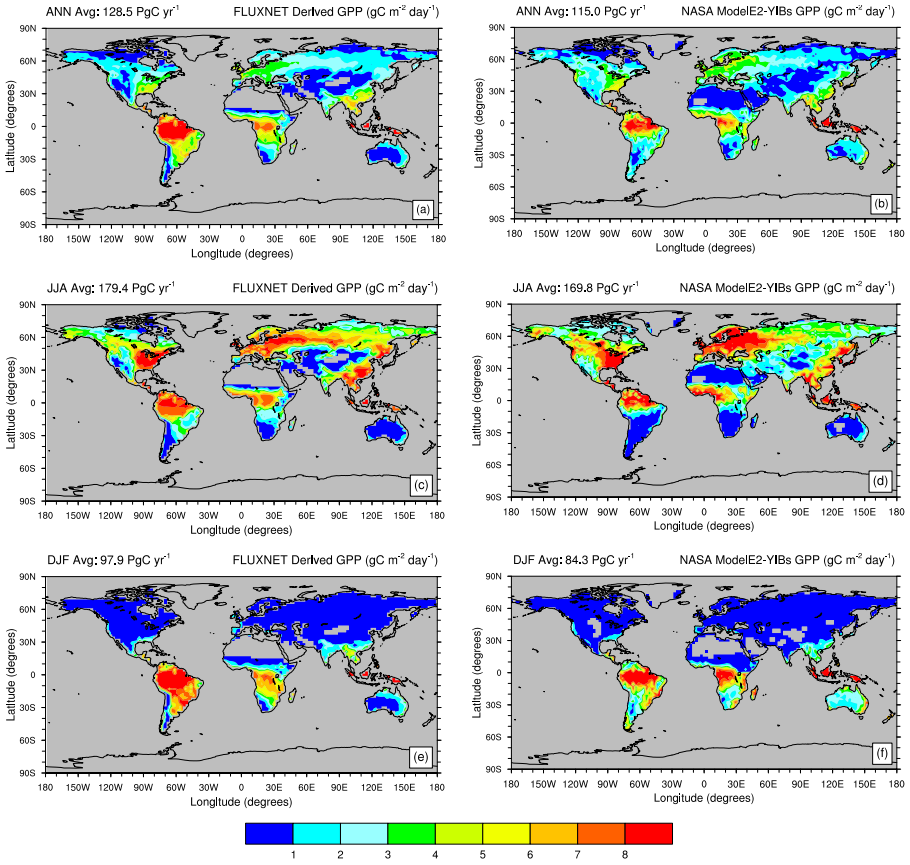

Figure 3. Annual and seasonal average gross primary productivity (GPP, in $g\,m^{-2}\,day^{-1}$) as seen by: **(a, c, e)** a global FLUXNET-derived GPP product (averaged over 2000–2011), and **(b, d, f)** NASA ModelE2-YIBS in the control present-day simulation (20 run years; ~ 2000s). Global mean values are given in the upper left corner of each map. Only boreal summer (JJA) and winter (DJF) seasonal averages are shown.

ACPD
15, 25433–25475, 2015

Sensitivity of photosynthesis and isoprene to aerosols

S. Strada and N. Unger

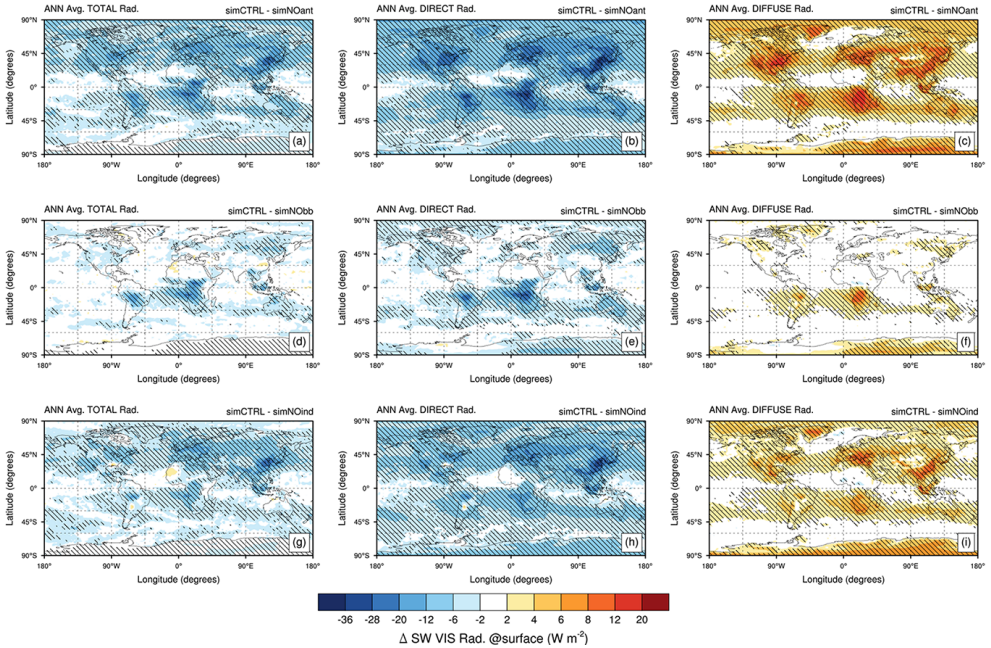

Figure 4. Spatial distribution of annual absolute change in short-wave visible (SW VIS) **(a, d, g)** total, **(b, e, h)** direct and **(c, f, i)** diffuse solar radiation (in $W\,m^{-2}$). Changes are computed between the control experiment (SimCTRL) and sensitivity experiments: **(a, c)** without all anthropogenic emissions (SimNOant); **(d, f)** without biomass burning emissions (SimNObb); and **(g–i)** without anthropogenic emissions except biomass burning (SimNOind). All experiments are set in a present-day climatic state. Shaded regions indicate areas where the change in solar radiation is significant at the 95 % confidence level. The difference has been computed using last 20 year averages for each experiment.

ACPD
15, 25433–25475, 2015

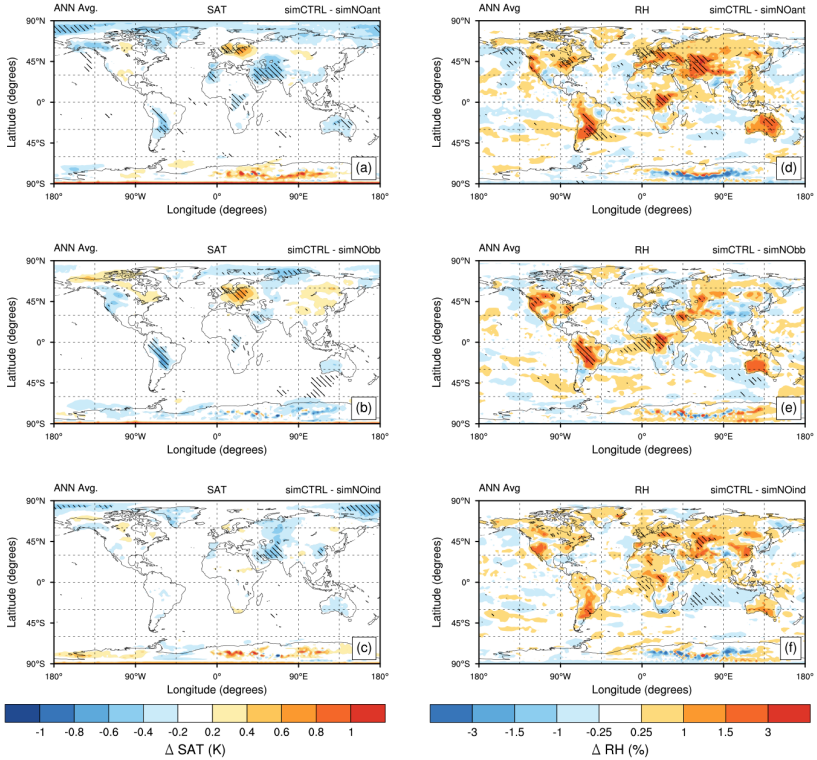

Figure 5. Spatial distribution of annual absolute change in surface atmospheric temperature (SAT, in K; left column panels) and relative humidity (RH, in %; right column panels) between the control experiment (SimCTRL) and sensitivity experiments: **(a, d)** without all anthropogenic emissions (SimNOant); **(b, e)** without biomass burning emissions (SimNObb); and **(c, f)** without anthropogenic emissions except biomass burning (SimNOind). All experiments are set in a present-day climatic state. Shaded regions indicate areas where the change in SAT (RH) is significant at the 95 % confidence level. The difference has been computed using last 20 year averages for each experiment.

ACPD
15, 25433–25475, 2015

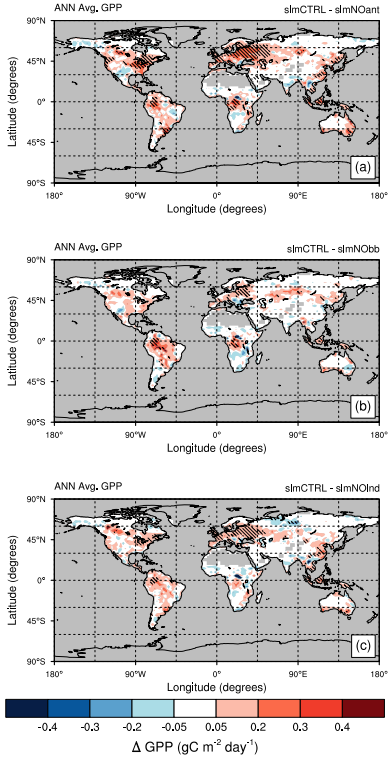

Figure 6. Spatial distribution of annual absolute change in Gross Primary Productivity (GPP, in $g\,C\,m^{-2}\,day^{-1}$) between the control experiment (SimCTRL) and sensitivity experiments: **(a)** without all anthropogenic emissions (SimNOant); **(b)** without biomass burning emissions (SimNObb); and **(c)** without anthropogenic emissions except biomass burning (SimNOind). All experiments are set in a present-day climatic state. Shaded regions indicate areas where changes in GPP are significant at the 95 % confidence level. The difference has been computed using last 20 year averages for each experiment.

ACPD
15, 25433–25475, 2015

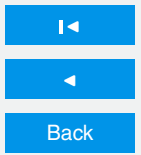

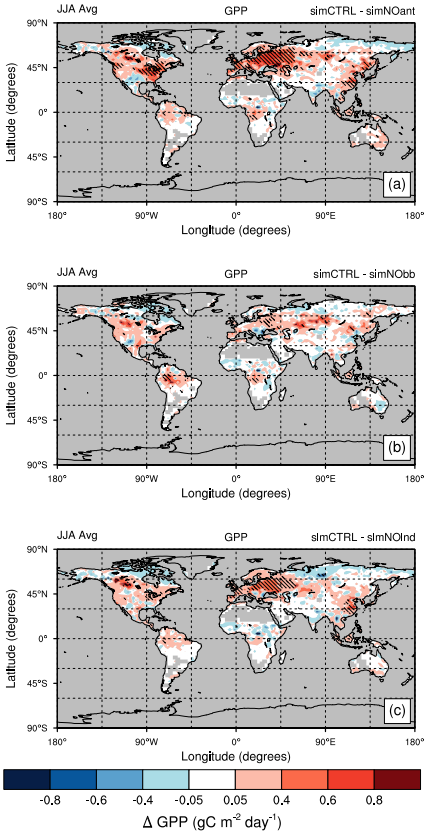

Figure 7. As Fig. 6 for seasonal (boreal summer) absolute change in Gross Primary Productivity (GPP, in $g C m^{-2} day^{-1}$) between the control experiment (SimCTRL) and sensitivity experiments: **(a)** SimNOant, **(b)** SimNObb and **(c)** SimNOind.

ACPD
15, 25433–25475, 2015

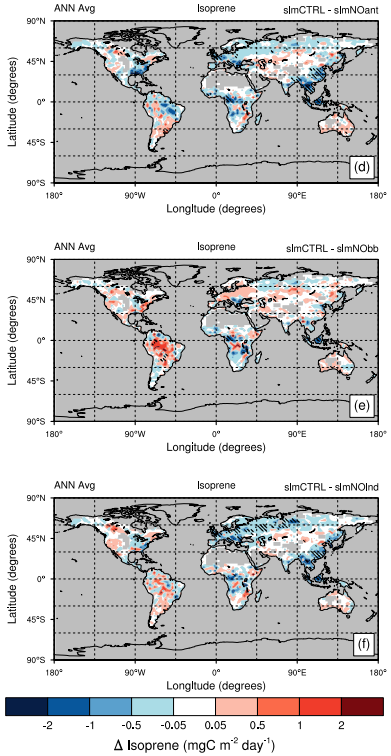

Figure 8. Spatial distribution of annual absolute change in isoprene emission (in $mg\,C\,m^{-2}\,day^{-1}$) between the control experiment (SimCTRL) and sensitivity experiments: **(a)** without all anthropogenic emissions (SimNOant); **(b)** without biomass burning emissions (SimNObb); and **(c)** without anthropogenic emissions except biomass burning (SimNOind). All experiments are set in a present-day climatic state. Shaded regions indicate areas where the changes in isoprene emission are significant at the 95 % confidence level. The difference has been computed using last 20 year averages for each experiment.

ACPD
15, 25433–25475, 2015

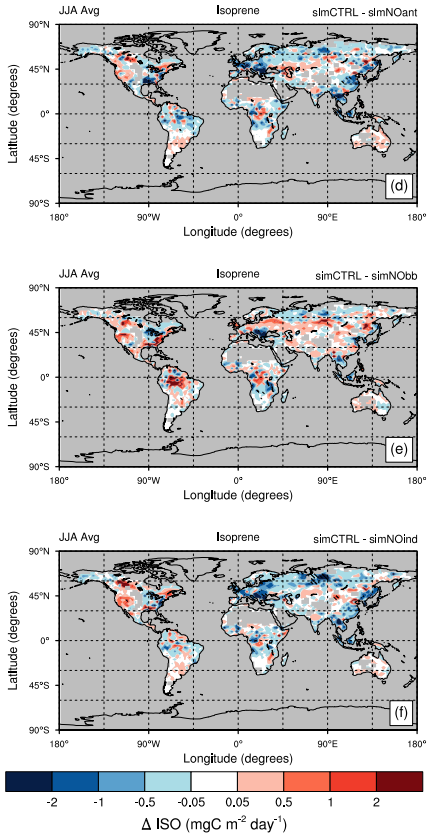

Figure 9. As Fig. 8 for seasonal (boreal summer) absolute change in isoprene emission (in $mg\,C\,m^{-2}\,day^{-1}$) between the control experiment (SimCTRL) and sensitivity experiments: **(a)** SimNOant, **(b)** SimNObb and **(c)** SimNOind.

ACPD
15, 25433–25475, 2015